International Journal for Uncertainty Quantification, 3 (3): 241–253 (2013)

SUMMARY VISUALIZATIONS FOR COASTAL SPATIAL-TEMPORAL DYNAMICS

Sidharth Thakur,[1,*] Laura Tateosian,[2] Helena Mitasova,[3] Eric Hardin,[4] & Margery Overton[5]

[1] *Renaissance Computing Institute, Raleigh, NC 27695*

[2] *North Caroline State University Center for Earth Observation, Raleigh, NC 27695*

[3] *North Caroline State University Department of Marine, Earth, and Atmospheric Sciences, Raleigh, NC 27695*

[4] *North Caroline State University Department of Physics, Raleigh, NC 27695*

[5] *North Caroline State University Department of Civil, Construction, and Environmental Engineering, Raleigh, NC 27695*

Original Manuscript Submitted: 03/01/2012; Final Draft Received: 28/09/2012

Digital scans of dynamic terrains such as coastal regions are now being gathered at high spatial and temporal resolution. Although standard tools based on geographic information systems (GIS) are indispensable for analyzing geospatial data, they have limited support to display time-dependent changes in data and information such as statistical distributions and uncertainty in data. We present a set of techniques for visually summarizing the dynamics of coastal dunes. We visualize summary statistics of important data attributes and risk or vulnerability indices as functions of both spatial and temporal dimensions in our data and represent uncertainty in the data set. We apply standard techniques, the space time cube and clustering, in novel ways to the domain of geomorphology. We combine surface-mapping and imagery with summary visualizations to retain important geographical context in the visualizations and reduce clutter due to direct plotting of statistical data in displays of geospatial information. We also address some issues pertaining to visualization of summary statistics for geographical regions at varying scales. We demonstrate visualization tools on time series of elevation models from the Outer Banks of North Carolina and observe temporal-spatial trends therein.

KEY WORDS: *uncertainty, visualization, geovisualization, glyph-based visualization, spatial-temporal analysis, space-time cube, coastal terrain, geomorphology, GRASS GIS, Outer Banks*

1. INTRODUCTION

Anthropogenic activity and natural processes modify land surface at various rates and scales, ranging from large gradual evolutions over the decadal time scale to events that can alter the local shape of land surfaces within days. Understanding this dynamic is essential for sustainable land use management, as well as disaster prevention and mitigation [1, 2].

Surveys of coastal regions based on light detection and ranging (LiDAR) technology over the past 15 years have generated a time series of elevation data at unprecedented resolutions. For the first time, this type of data is available as a regional, multiyear time series, providing an opportunity for transition from traditional, static representation of topography to terrain abstraction as a three-dimensional dynamic layer. Supporting effective analysis for this type of data presents challenges for visualization.

*Correspond to Sidharth Thakur, E-mail: sthakur@renci.org

2152–5080/13/$35.00

Although standard raster-based analysis provides unique insights into patterns of topographic change, it does not fully capture the spatial complexity of elevation dynamics, especially when considering attributes that combine vertical change with horizontal migration. Moreover, traditional two- and three-dimensional geospatial visualization tools often lack support to display important data attributes such as statistical distributions, error, and uncertainty.

We present a collection of summary visualizations that can expose spatial-temporal changes in dynamic coastal regions. Summarization provides several benefits for this high-resolution, multiple time step, large spatial extent data. We use it to reduce data density, while preserving salient characteristics and important patterns. Standard GIS raster-based analysis of large, dense, multitemporal data can overwhelm the viewer. Summarization provides overview within spatial context. Summarizations facilitate discovery or confirmation of patterns and relationships in elevation time series.

Our visualizations are intended as tools to supplement analysis, enabling domain scientists to explore and discover fluctuations in coastal features such as dune ridge elevation and migration and the effects of terrain-altering events. The main contribution of this paper is a collection of geospatial visualizations that apply standard and novel visual techniques to represent summary and uncertainty information for rich coastal terrain dynamics data sets.

The remainder of this paper is organized as follows: Section 2 describes background and related work. Sections 3 and 4 present techniques we are using to display summary statistics and uncertainty for dynamic terrain. Sections 5 and 6 discuss our findings and directions for future work.

2. BACKGROUND AND RELATED WORK

Coastal North Carolina has a unique geography with its long narrow strip of "barrier islands" called the *Outer Banks* sitting a few miles out in the Atlantic Ocean. Along the Outer Banks there are features of sand close to the beaches called *fore dunes*, which exhibit dynamic behavior such as lateral migration and changes in elevation (Fig. 1) [3]. The shape of the fore dune profiles changes constantly due to waves and wind; natural phenomena such as hurricanes and storm surges can alter the shape drastically. Storm events such as Hurricanes Isabel (2003) and Irene (2011) underline the vulnerability and dynamic nature of coastal terrain; Fig. 2 shows a site in the Outer Banks where breaks in the

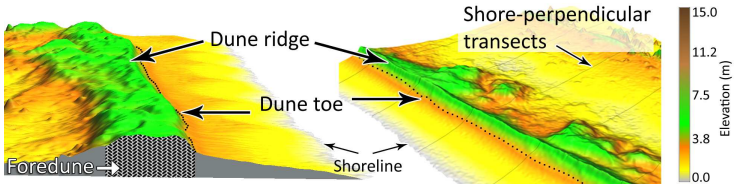

FIG. 1: Beach anatomy: the dune ridge—the highest elevation on the dune, fore dune—the dune closest to the ocean, beach profile (left) as sliced by a transect, transects (right) perpendicular to the shoreline.

FIG. 2: New breaks in the North Carolina Outer Banks caused by Hurricane Irene in August 2011.

island occurred due to Hurricane Irene. Due to storm surges, the water level can rise above the dune ridge and wash over the dune causing vulnerability to breaching. Analyzing these changes is important because these fore dunes act as flexible barriers to storm surges and waves, protecting low-lying back shore areas, and helping to preserve the low barrier islands.

Domain scientists routinely use LiDAR terrain scans to study coastal processes and to understand spatio-temporal changes in the small- and large-scale features found in coastal areas. Due to the increasingly high resolutions at which coastal LiDAR data are now gathered, it has become more challenging for the community to effectively visualize important properties of the data such as the uncertainty in representing multitemporal data using statistical summarization.

The focus of our work is to develop summary visualizations of the dynamics of coastal terrains to address some of the challenges introduced by the availability of large coastal terrain data sets. We use 11 digital elevation models (DEMs) of the Outer Banks derived from LiDAR geographically registered surveys at 11 distinct time steps over the last decade. Each LiDAR data set is an (x, y, z) point cloud composed of points interpolated at a 0.5-m resolution to create a DEM [4]. U.S. Geological Survey (USGS) transects, lines perpendicular to shoreline (see Fig. 1), are also used in some cases to sample the data.

Summarization of the spatial-temporal changes in coastal features can be useful for visualizing salient behavior of this dynamic coastal region. In this work, we also handle uncertainty introduced by the summarization process by visualizing spatial and temporal distributions of statistical information in our data.

Extensive related work has addressed challenges in dealing with uncertainty and error in geospatial-temporal data. Pang et al. pioneered efforts to augment standard geovisualizations with information about error and uncertainty in the underlying data; this work proposes combinations of two- and three-dimensional graphical techniques and animations [5–7]. MacEachren et al. review many aspects of dealing with uncertainty in geovisualization, such as conceptualizing uncertainty, typology of uncertainty for geospatial data, visual representation of uncertainty parameters, and usability of tools for integrating uncertainty visualization into standard GIS analytical approaches [8]. Johnson et al. review state-of-the-art techniques in visualizing uncertainty and describe challenges relating to effective uncertainty visualization for scientific data sets [9]. Laskey et al. present a probabilistic ontology to manage and propagate uncertainty in the data designed to standardize treatment of uncertainty in GIS [10].

Other work has focused on uncertainty visualization within specific spatial data domains. For example, Li et al. describe glyph-based approaches to visualize uncertainty in astrophysical data [11]. Sanyal et al. visualize uncertainty in ensembles of meteorological data on hurricane paths [12]. In [13] user studies evaluate uncertainty visualization for one- and two-dimensional data. In a recent workshop, practitioners and researchers from a variety of science and engineering fields discussed uncertainty as it relates to representation, quantification, propagation, and visualization of uncertainty [14].

Uncertainty visualizations have also been developed to support analysis in traditional GIS. For example, Wood et al. discuss error during the generation of digital elevation maps and various GIS-based approaches for visualizing uncertainty-related quantities of error, accuracy, and data quality [15]. Hengl uses a Hue-Saturation-Intensity color-based scheme to augment traditional GIS maps to visualize uncertainty in soil characteristics stream networks extracted from DEMs [16–18].

Data summarization approaches have been applied to visualizing geospatial-temporal data. Hoeber et al. display changes in North Atlantic cod populations over time using a combinatorial visualization of regional difference maps [19]. Potter et al. identify a set of summary statistics to abstract key attributes of large, spatial multivariate data sets and visualize summary and uncertainty using modified box plots [20]. Another approach is based on isosurfaces to visualize terrain dynamics. For example, recent work has begun to use isosurfaces to visualize terrain geomorphology [3, 21]. This technique uses a space-time voxel model to represent a time series of digital elevation data as a continuous trivariate function $z = f(x, y, t)$, where (x, y), the horizontal location and t, time, determine the elevation value, z. Isosurfaces are useful to display properties of fore dunes such as stable, preserved peaks and significant losses due to storm action.

Other approaches to summary visualization use data mining techniques such as clustering to obtain spatial-temporal clusters of geospatial regions that have similar spatial or spatial-temporal distributions of multivariate data. For example, Bordoloi et al. cluster spatial distributions of probability density functions for forest cover data and

employ feature extraction and visualization to analyze the data sets at varying levels of granularity [22]. Love et al. compute interpoint similarity and use contours, streamlines, and isosurfaces to visualize uncertainty in multivariate geospatial data sets [23].

We next describe our methods to develop summary visualizations of coastal terrain dynamics.

3. VISUALIZATION OF STATISTICAL INFORMATION

Statistical information about terrain attributes is useful for summarizing complicated dynamics and understanding changes in the attributes over both space and time. We employ several types of plots to visualize statistical information and to provide overviews of changes in terrain data. Changes over time are an important component of terrain analysis. The lateral and vertical movement of important features such as dune ridge lines can be an indicator of vulnerability. Plots of these lines for all of the time steps in 3D Cartesian coordinate space are difficult to interpret so we look to a 3D visualization approach called *space-time cubes* (STC) [24]. STCs use two dimensions of a cube (i.e., x, y directions) to display spatial context and the third (the z direction) to display the temporal domain, instead of elevation.

Displaying important features in large regions of data sets such as these can pose a challenge. In the case of the North Carolina (NC) Outer Banks, the long, narrow geography of the land mass makes it difficult for traditional approaches to display terrain attributes while maintaining a geospatial context.

To address the challenge of providing an overview of a large region, we have adapted standard plots used by USGS to display quantitative data for long shorelines and barrier islands [25]. The USGS plots colored bands parallel to the shore to represent quantitative data, such as potential for inundation for various storm severities, at corresponding long shore locations. We enhance this layout, combining this idea with the STC concept to display a variety of statistical data for the NC Outer Banks.

A typical visualization using our approach is the plot of mean and standard deviation shown in Fig. 3. In this example, stacked bar charts (brown for mean and tan for standard deviation) are used to represent statistical data about

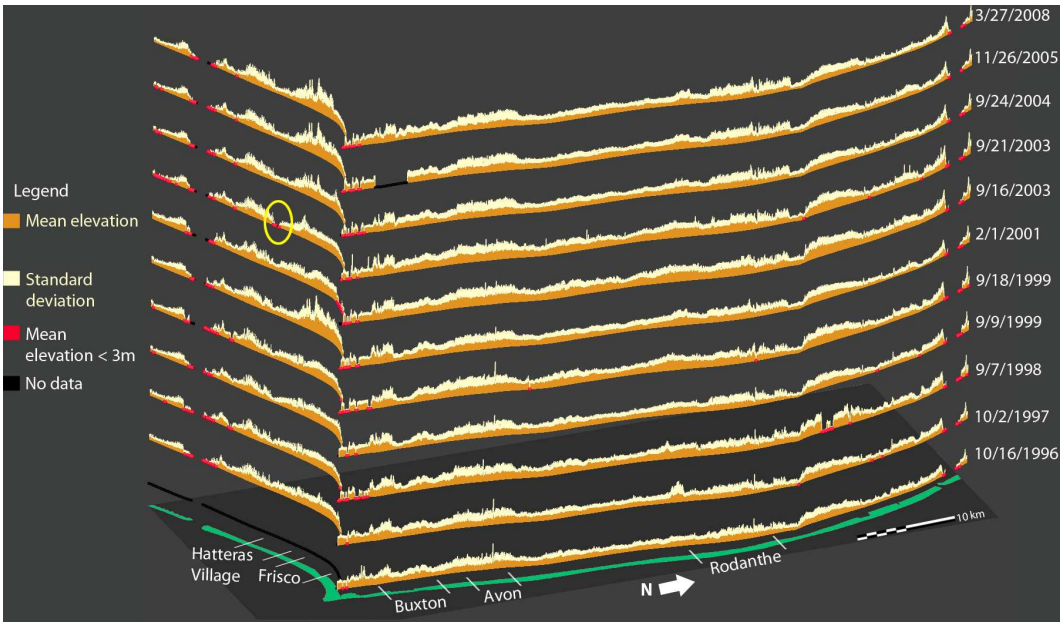

FIG. 3: Terrain elevations of North Carolina barrier islands 1996–2008. Stacked bar charts display mean elevation (brown) and standard deviation (tan) for areas between transects. Bar charts for each time step in the data are drawn parallel to the shoreline to display spatial and temporal variation in elevations along a stretch of the Outer Banks (about 75 km long). The barrier islands used for these calculations are shown in green along the bottom. The yellow circle highlights a breach caused by Hurricane Isabel in 2003.

elevations for a large portion of the Outer Banks (about 75 km in length). The data set pertains to about 3000 zones between pairs of transects sampled from the 11 time step DEM series. This illustrates average elevation and standard deviation for each zone. This extent includes the towns of Hatteras Village, Frisco, Buxton, Avon, and Rodanthe. Patches of high standard deviations recurring at each time step are due to buildings in these developed areas. Pea Island National Wildlife Refuge, north of Rodanthe, has a large stretch of consistently high mean elevation across time, due to large maintained dunes in the refuge, whereas, low means in undeveloped areas could indicate areas with low or narrow dunes. Pink point markers in Fig. 3 highlight areas with average elevation below 3 m. Low-lying areas such as the dunes circled in yellow in Fig. 3 can be vulnerable to overwash; here Hurricane Isabel breached Hatteras Island.

3.1 Ridge Line Summary and Uncertainty Visualization

When storms hit, fore dunes can act as barriers preventing overwash and breaches. Therefore, fore dune ridge elevation trends are an important factor for characterizing storm vulnerability. We present visualizations for summarizing ridge elevation and differences in elevations and then we visualize ridge elevation uncertainty.

Figure 4 uses a row of spheres for each time step where sphere size represents dune ridge elevation. Though STCs have previously been used to display many types of data that have both spatial and temporal components, to our knowledge, STCs have not been used for terrain elevation visualization, but have several useful features for this application. Properties of the time dimension, such as gaps in observed data and unequal intervals can be displayed more explicitly in an STC-based representation than in standard two-dimensional visualizations. For example, no 2006–2007 Outer Banks DEMs were available for Fig. 4. STC displays can combine visualizations of time-varying quantitative terrain attributes with raster maps and orthographic images for useful contextual information. A 2009

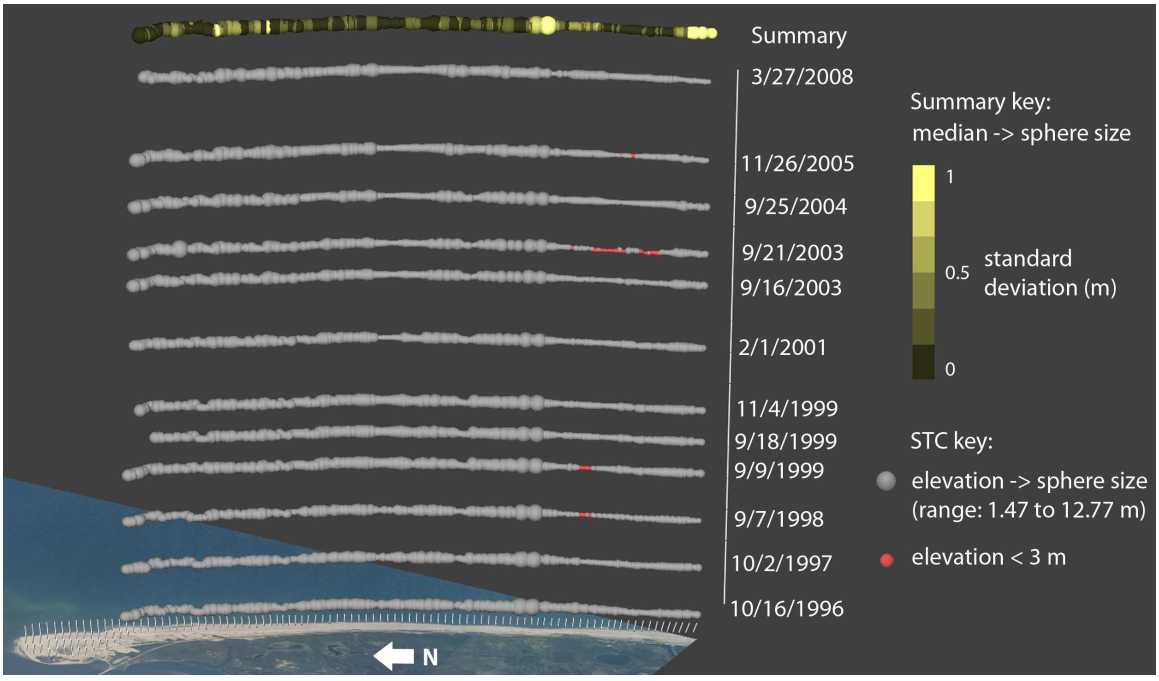

FIG. 4: Visualizing ridge line elevations and changes in elevation south of the Oregon Inlet. Each line of gray spheres displays the conditions at the labeled time step. Spheres are positioned along the ridge in the horizontal plane. Sphere size represents ridge line elevation as sampled by intersecting transects. The size of the spheres in the top line show the median elevation over time with color representing standard deviation. Locations on the fore dune that experienced severe loss in elevation are shown using red spheres.

orthographic image shows the ocean and land formations of Oregon Inlet in Fig. 4. Also, using STCs enables us to depict changes in spatial and temporal attributes of geospatial data in a single interactive display. To show ridge line movement, the (x, y) sphere positions correspond to the fore dune ridge location on the 2D Oregon Inlet image.

Figure 5 visualizes pairwise differences in time steps, starting with the difference between 10/16/1996 and 10/2/1997 in the bottom row. The height of the cones represents the magnitude of the difference. Tan to red cones point upward for increases in ridge line elevation; blue cones point downward for decreases. Median differences are shown in the top row with cone color and height. Comparison of terrain before and after terrain-altering events, such as Hurricane Isabel between 9/16/2003 and 9/21/2003, reveals regions with losses followed by large gains, which may reflect dune maintenance efforts.

As mentioned before, the ridge lines of fore dunes provide important clues to vulnerability due to storm surge or wind action. For example, position and elevation are important parameters that determine the degree of vulnerability or impact of storms, which is communicated using a standard notation called the storm impact scale [26]. It is therefore important to visualize uncertainty and error in ridge line position. We next describe a visualization of this type of information.

A new technique to automatically extract the ridge line of a fore dune from a coastal DEM uses a computational process known as least-cost path extraction (LCP) [26]. Because there is inherently some uncertainty in the DEM which is derived by interpolation from a LiDAR survey, there is also uncertainty in the ridge line being extracted. To simulate this uncertainty in position and elevation of ridge lines obtained using the LCP method, Gaussian noise with standard deviation equal to predictive DEM error is added to a DEM and then the ridge line is extracted. Repeating this 1000 times, we obtained ridge lines from 1000 different instances of DEMs with noise and visualize the results to communicate uncertainty in the extracted ridge lines.

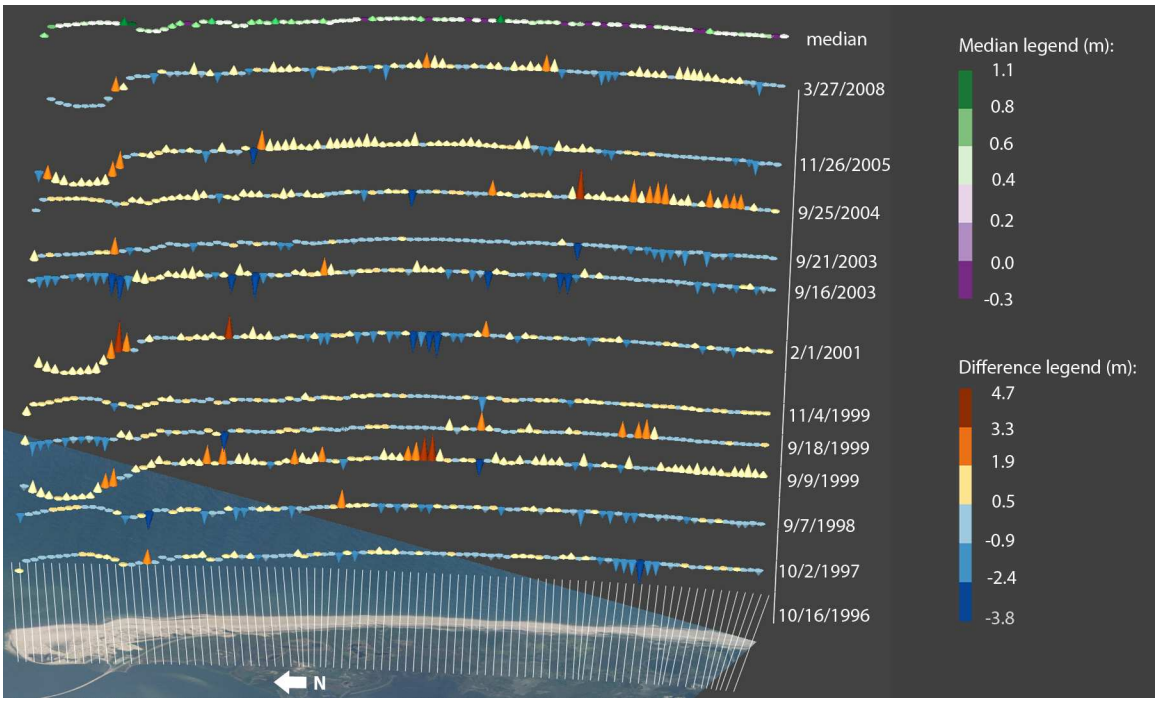

FIG. 5: Visualizing ridge line elevation changes in elevation south of the Oregon Inlet. Pairwise differences in ridge line elevation south of Oregon Inlet. The line of cones at each time step display the difference in ridge line elevation from the previous time step: cone direction indicates an increase (up) or decrease (down) in elevation, cone height represents magnitude of the difference, and cone color corresponds to the value of the difference. The purple-green cones along the top show the median difference over all time steps.

Figure 6 shows a visualization of total uncertainty along a fore dune using a glyph-based approach. The glyph is a continuous, symmetrical curve plotted above the fore dune. Height of the curve in the vertical direction denotes the magnitude of uncertainty of elevation of points on the fore dune; thickness of the curve represents uncertainty in determining horizontal position of a ridge line. We observed maximum uncertainty of about 40 cm in elevation of ridge lines. Uncertainty in horizontal position was found to be around 1–2 m, which is close to the horizontal accuracy of LiDAR; hence horizontal uncertainty is still small but larger than the uncertainty in the z direction (elevation). However, vertical uncertainty is treated in our analysis because the height of the dune is the topographic parameter used in the storm impact scale [26].

4. CLUSTERING TIME SERIES

Dynamic terrains such as coastal regions often exhibit changes to surface features such as shoreline and sand dunes. Hurricanes can abruptly cause drastic alterations to these landscapes in a very short time, but natural processes also change surface features gradually over longer time periods. To help us understand these longer-term phenomena we create visualizations that provide overviews of spatial-temporal changes in dynamics of coastal terrain.

4.1 Clustering Approach

To generate spatial-temporal overviews, we cluster points, with each point representing a time series of elevations sampled at that point on terrain raster maps for each time step. Clustering can reveal useful information such as spatial and temporal distributions of regions with similar temporal dynamics, which can be difficult to obtain using standard approaches.

In our clustering method, we use a quantitative similarity measure of changes in elevation over time to compute similarity between time series of points sampled on a terrain. A variety of similarity measures have been developed to extract patterns in time-dependent data [22, 23, 27, 28]. Here we apply three similarity measures: Pearson correlation, a custom squared-distance error function, and a qualitative measure for comparing short time series. See Table 1 in Appendix A.

We compute similarity scores between elevation time series of all unique pairs of points sampled on a terrain. We then use multidimensional scaling (MDS) to generate a plot of similarity relationships [29]. MDS takes as input an $N \times N$ matrix of pairwise similarity scores and produces a two-dimensional "scatter plot." Each point in the plot corresponds to the elevation time series at some point on the terrain and proximity of points in the plot represents

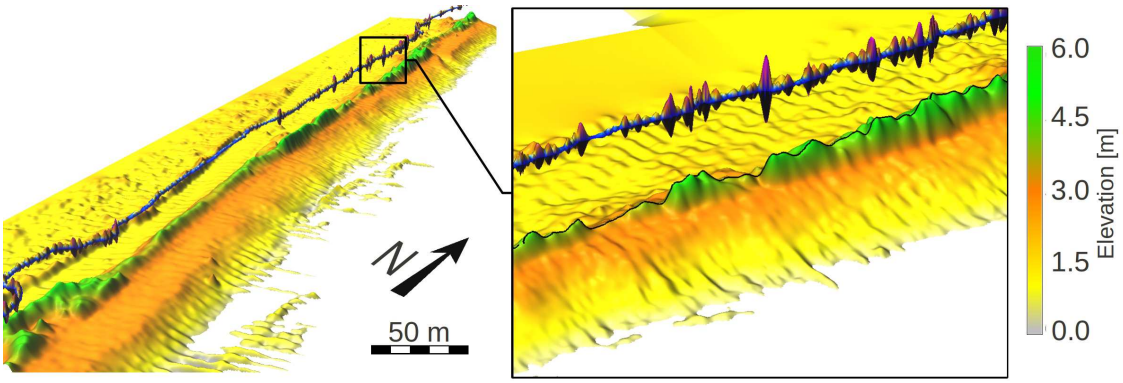

FIG. 6: Uncertainty of the ridge line obtained from 1000 different instances of DEMs of a section of Outer Banks, North Carolina. A selected ridge line (black) is drawn on the yellow-green fore dune (drawn with 3x elevation exaggeration). The blue-pink uncertainty volume drawn 10 m above the model shows the alternate elevations and lateral positions assumed by ridge lines from the 1000 DEM collection. The elevation of the uncertainty volume is drawn with 9x elevation exaggeration.

similarity among corresponding terrain points. The MDS plot thus provides a means to obtain similarity among areas on a terrain over all time steps.

After the MDS plot is generated, we use k-means to partition point clusters in the plot into a set of k clusters. The MDS points are colored by cluster and the colored points are redrawn in their original geospatial locations and displayed with an underlying map or terrain image for context.

Figure 7 demonstrates this technique on the region south of the NC Outer Banks Oregon Inlet. Clusters found using the k-means algorithm are color coded according to relative magnitude of the cluster mean elevation. Data for the clustering examples were derived from elevations of points (more than 10,000) sampled on raster maps at a resolution of 10 m. The data correspond to 11 time steps sampled at unequal intervals over the past decade (1996–2008).

The clusters found using the three metrics denote different regimes in Oregon Inlet that have similar elevation time series based on the chosen metric. The three colors in Figure 7(a) represent regions such as beach and other areas with small overall elevations (orange), higher-elevation areas such as slopes of fore dunes (pale yellow), and fore dune ridge (red). For this data set, values of k between 3 and 6 yield the most interesting results.

Higher values of k in the k-means algorithm, such as k = 6 to 9, produce clusters having lower within-cluster error, that is, smaller variance between means of elevation time series of points in a cluster and corresponding cluster mean. For example, Fig. 7(b) shows a clustering result for squared error measure with $k = 6$. Clustering results for larger values of k (that is, $k \geq 6$) are not very useful because differences between one or more clusters may not be significant. Moreover, when the number of clusters is large it is difficult to associate meaningful regimes with the individual small-sized clusters. For example, unlike the visualization in Fig. 7(a), which has three different regimes found using $k = 3$, it is difficult to distinguish the six regimes in Fig. 7(b) found using $k = 6$.

Figure 7(c) shows a clustering result using a qualitative metric [Eq. (A.2) in Table A.1]. The clusters in the figure represent a group of points whose time series had similar shapes; that is, points within the same cluster underwent similar changes irrespective of the magnitude of the change. Finally, Fig. 7(d) shows a clustering of points based on the standard Pearson correlation metric [Eq. (A.3) in Table A.1], which compares linear relationships among a set of data series.

The three metrics produce clusters with some common features. For example, regions with low elevations such as beaches and a road parallel to the shore can be readily identified in clusters with lowest mean elevations. There are differences among the clustering results as well. The shapes of the MDS scatter plot (shown in insets in the figures) are qualitatively different from one another. For example, the scatter plots for the squared error metric and Pearson correlation [Figs. 7(a) and 7(c) respectively] are elongated and have clear separation among elevation time series of the points sampled around the Oregon Inlet region. Conversely, the scatter plot for qualitative measure [Fig. 7(b)] is globular and it may be difficult using the k-means algorithm to obtain clusters with significant differences. In fact, the qualitative metric produces clusters with the lowest average intercluster difference between cluster means (average intercluster difference: squared error metric = 3.07 m, Pearson correlation = 0.98 m, and qualitative measure = 0.6 m) and also with lowest root mean square difference (RMSD) between cluster means (RMSD between intercluster means: squared error metric = 5.66 m, Pearson correlation = 1.81 m, and qualitative metric = 1.17 m).

4.2 Visualization of Error

As described earlier in this section, clustering results vary based on the choice of similarity metric used for clustering the elevation time series and the choice of number of partitions used to partition MDS scatter plots. Because the elevation time series of points are assigned to one cluster or another, there is error introduced within each cluster due to the partitioning procedure. We treat the error as the variance between means of elevation time series of points in a cluster relative to the overall mean of the corresponding cluster. This within-cluster error is visualized as the standard deviation of means of elevation time series within each cluster.

Figure 8 illustrates our approach to visualize error within each cluster. We draw a sphere for each point along a vertical axis, which represents mean elevation of the elevation time series at that point. A line from the sphere to a horizontal plane representing the mean of the parent cluster shows how different that point's mean is from its cluster

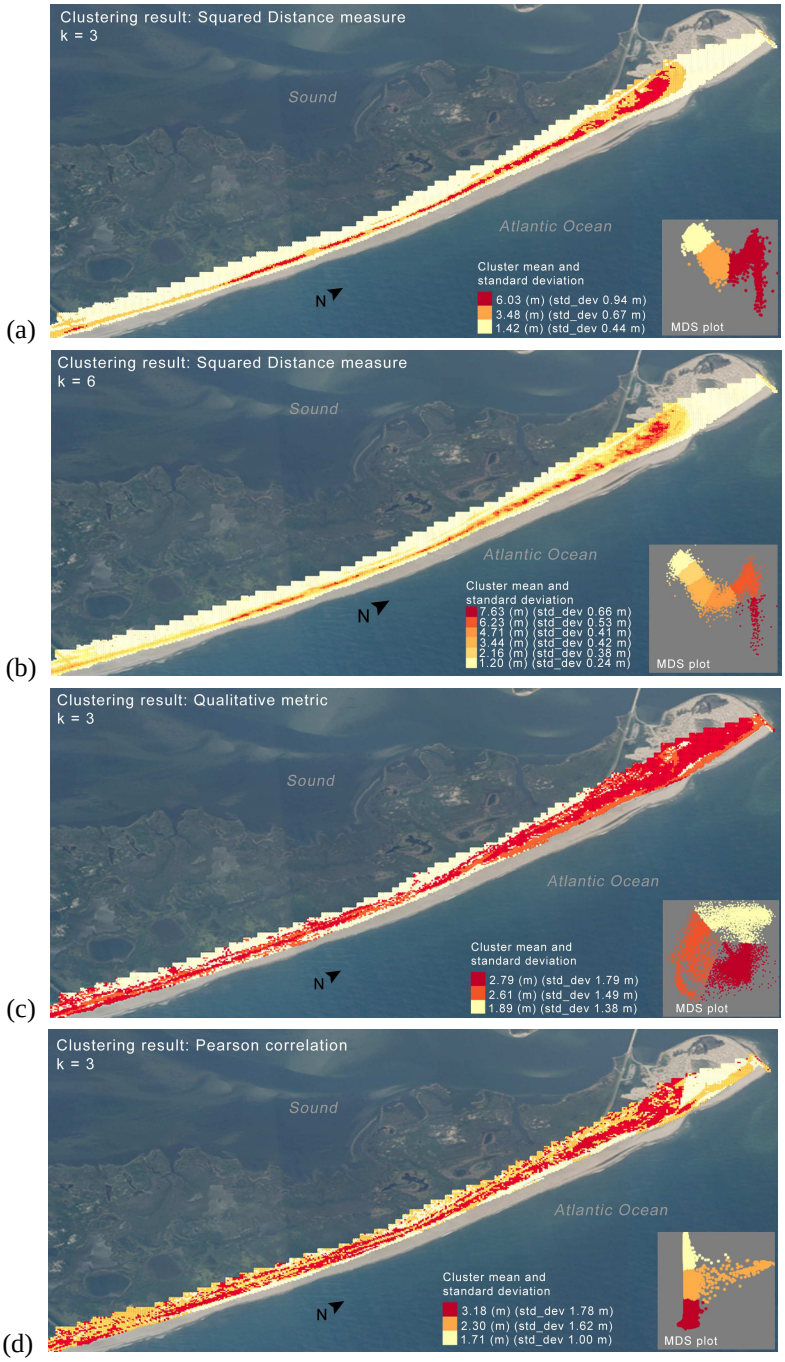

FIG. 7: Results of clustering elevation time series for Oregon Inlet region in NC Outer Banks islands using three different similarity measures. (a) and (b) Clustering result using the distance measure in Eq. (A.1) and using two different values of k, that is, $k = 3$ and $k = 6$. (c) Clustering result using the qualitative measure in Eq. (A.2). (d) Clustering result using the standard Pearson correlation measure. See Appendix A for details of these measures. The MDS scatter plots in inset show, similarity relationship among all points in the data set. There are about 10,000 points in the data set used to generate these examples. Clusters of points in the plot and on the map of the terrain are color coded according to increasing values of mean elevation of the clusters.

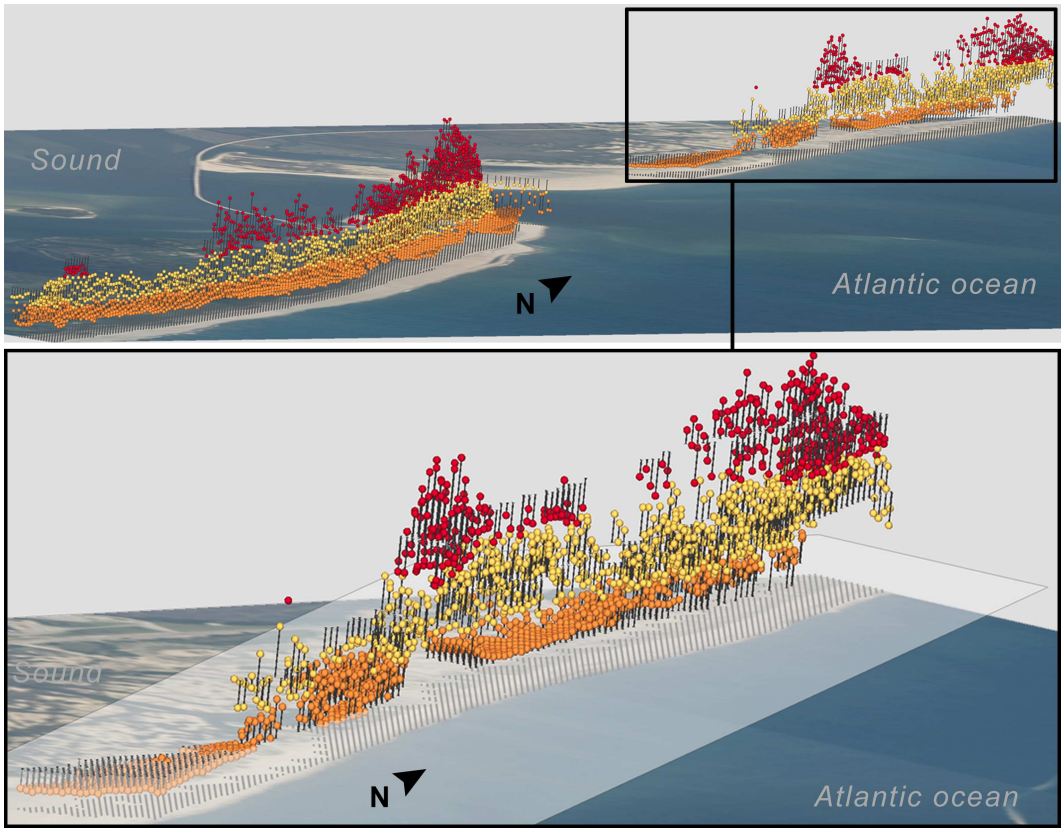

FIG. 8: Visualization of error within each cluster of elevation time series. Vertical position of spheres (color coded by their cluster IDs) indicate mean elevations of points at corresponding x-y location on the map. A semi-transparent plane (white plane in bottom figure) represents the mean of the cluster of points shown in orange. Black lines from the spheres to the semi-transparent plane indicate the difference between means of each point and the cluster mean.

mean. Other information such as one standard deviation above and below a cluster's mean value can be displayed optionally.

5. DISCUSSION AND FUTURE WORK

Our STCs reveal trends in elevation and ridge lines over time. We see trends of consistently low mean areal elevation, followed by breaches in these locations. We also saw analogous patterns in ridge line elevation. The ridge line elevations show decreases after storms where breaches occurred. This was followed by large increases which may be due to dune recovery or reconstruction. The dune ridge uncertainty visualization serves to display variations that exist in ridge lines and other derived elevation features due to the uncertainty in the elevation models.

With clustering, we identified and visualized areas which had common elevation over time or common elevation trends over time. Our approach is to use a similarity measure to determine pairwise similarity relationships among points in a region. We use multidimensional scaling (MDS) to visualize the similarity relationships and to extract clusters of points with similar time series. We applied our clustering approach to points sampled on a region around Oregon Inlet, a natural opening in North Carolina Outer Banks. Clustering can be useful for confirming profile-based analysis of beach areas. It also shows that some areas have very different average elevations but have similar loss/gain trends. This could imply that wind is more influential than wave action in these regions. Other more-sophisticated clustering approaches need to be tried to extract more complicated patterns.

We have addressed some challenges in visualizing spatio-temporal changes in dynamic coastal regions. Our primary approach is to create summary visualizations of changes in elevation and areas of regions based on data derived from LiDAR scans of the terrain. We also focus on visualization of error, which is introduced in the visualizations due to summarization of the data.

Although we have dealt with spatio-temporal distributions for elevation and areas, other terrain attributes can be visualized using our approach. Some of these attributes include positions of shoreline and fore dunes, width of beaches, and vulnerability along the coastline.

The techniques discussed here were developed in collaboration with domain scientists (co-authors) and the methods presented have some user feedback built in. However, controlled task-based user evaluations are needed, though they are beyond the scope of this work. In our ongoing work, we are also exploring other methods to summarize coastal dynamics. One promising approach is to use isosurfaces to explore specific types of phenomena such as dune overwash and rebuilding of fore dune ridges.

6. CONCLUSION

We discuss summary-based visualization approaches to explore the dynamics of coastal regions in North Carolina Outer Banks. One approach we use is to display statistical information about spatio-temporal changes in elevation and areas of coastal regions based on data derived from high-resolution LiDAR scans of the terrain. We employ a number of different types of plots to display the spatio-temporal changes and uncertainty introduced by the summarization process. One of the plots we use is based on a standard plot used by USGS to display data for shorelines and barrier islands. Our modified plot allows us to display in a single pictorial overview the elevation time series and variations for a large geographic region. Another technique we use is based on clustering time series of elevations of points sampled on a terrain. This approach allows us to abstract salient spatio-temporal patterns in a region and create a visual summary of some aspects of the terrain dynamics.

REFERENCES

1. Zhou, G. and Xie, M., Coastal 3D morphological change analysis using LiDAR series data: A case study of Assateague Island National Seashore, *J. Coastal Res.*, 25:435–447, 2009.
2. Mitasova, H., Harmon, R., Weaver, K., Lyons, N., and Overton, M., Scientific visualization of landscapes and landforms, *Geomorphology*, 13(1):122–137, 2012.
3. Mitasova, H., Overton, M. F., Recalde, J. J., Bernstein, D. J., and Freeman, C. W., Raster-based analysis of coastal terrain dynamics from multitemporal LiDAR data, *J. Coastal Res.*, pp. 507–514, 2009.
4. Mitasova, H., Hardin, E., Kurum, M., and Overton, M., Geospatial analysis of vulnerable beach-foredune systems from decadal time series of LiDAR data, *J. Costal Conservation, Manag. Planning*, 14(3):161–172, 2010.
5. Pang, A., Wittenbrink, C. M., and Lodh, S. K., Approaches to uncertainty visualization, *Visual Comput.*, 13:370–390, 1996.
6. Pang, A., Visualizing uncertainty in geo-spatial data, In *Proceedings of the Workshop on the Intersections between Geospatial Information and Information Technology*, 2001.
7. Pang, A., Visualizing uncertainty in natural hazards, In: Bostrom, A., French, S., Gottlieb, S., Covello, V. T., Mumpower, J., Spicker, S. F., and Stallen, P.-J. M. (Eds.), *Risk Assessment, Modeling and Decision Support*, Vol. 14, Technology, Risk, and Society, Springer, Berlin, Heidelberg, pp. 261–294, 2008.
8. MacEachren, A. M., Robinson, A., Hopper, S., Gardner, S., Murray, R., Gahegan, M., and Hetzler, E., Visualizing geospatial information uncertainty: What we know and what we need to know, *Cartography Geographic Information Sci.*, 32(3):139–160, 2005.
9. Johnson, C. and Sanderson, A., A next step: Visualizing errors and uncertainty, *Comput. Graphics Appl., IEEE*, 23(5):6–10, 2003.
10. Laskey, K. B., Wright, E. J., and Costa, P. C. G. D., Envisioning uncertainty in geospatial information, *Int. J. Approximate Reasoning*, 51:209–223, 2007.

11. Li, H., Fu, C.-W., Li, Y., and Hanson, A., Visualizing large-scale uncertainty in astrophysical data, *IEEE Trans. Visualization Comput. Graphics*, 13(6):1640–1647, 2007.
12. Sanyal, J., Zhang, S. n., Dyer, J., Mercer, A., Amburn, P., and Moorhead, R. J., Noodles: A tool for visualization of numerical weather model ensemble uncertainty, *IEEE Trans. Visualization Comput. Graphics*, 16(6):1421–1430, 2010.
13. Sanyal, J., Zhang, S., Bhattacharya, G., Amburn, P., and Moorhead, R., A user study to compare four uncertainty visualization methods for 1D and 2D datasets, *IEEE Trans. Visualization Comput. Graphics*, 15(6):1209–1218, 2009.
14. Johnson, C. and Pang, A., Working with uncertainty workshop: Representation, quantification, propagation, visualization, and communication, In *Proceedings of IEEE VisWeek Visualization Conference*, Providence, Rhode Island, 2011.
15. Wood, J. and Fisher, P., Assessing interpolation accuracy in elevation models, *Comput. Graphics Appl., IEEE*, 13(2):48–56, 1993.
16. Hengl, T., Heuvelink, G. B. M., and Loon, E. E.v., On the uncertainty of stream networks derived from elevation data: The error propagation approach, *Hydrol. Earth System Sci. Disc.*, 7(1):767–799, 2010.
17. Hengl, T., Visualisation of uncertainty using the HSI colour model: Computations with colours, In *Proceedings of the 7th International Conference on GeoComputation*, CD-ROM, p. 817, 2003.
18. Hengl, T. and Toomanian, N., Maps are not what they seem: Representing uncertainty in soil-property maps, In *Proceedings of the 7th International Symposium on Spatial Accuracy Assessment in Natural Resources and Environmental Sciences*, Lisbon, Portugal, Instituto Geográphico Português, pp. 805–813, 2006.
19. Hoeber, O., Wilson, G. C., Harding, S., Enguehard, R., and Devillers, R., Exploring geo-temporal differences using GTdiff, In *Proceedings of IEEE Pacific Visualization Symposium*, pp. 139–146, 2011.
20. Potter, K., Kniss, J., Riesenfeld, R., and Johhson, C. R., Visualizing summary statistics and uncertainty, In *Computer Graphics Forum (Proceedings of EuroVis 2010)*, Vol. 29, pp. 823–831, 2010.
21. Starek, M., Mitasova, H., Hardin, E., Overton, M., and Harmon, R., Modeling and analysis of landscape evolution using airborne, terrestrial, and laboratory laser scanning, *Geosphere*, 7:1340–1356, 2011.
22. Bordoloi, U., Kao, D. L., and Shen, H., Visualization techniques for spatial probability density function data, *Data Sci. J.*, 3:153–162, 2004.
23. Love, A. L., Pang, A., and Kao, D. L., Visualizing spatial multivalue data, *IEEE Comput. Graph. Appl.*, 25:69–79, May 2005.
24. Kraak, M., The space-time cube revisited from a geovisualization perspective, In *Proceedings 21st International Cartographic Conference*, pp. 1988–1995, 2003.
25. Stockdon, H. and Thompson, D., Vulnerability of national park service beaches to inundation during a direct hurricane landfall: Fire island national seashore, *USGS Open File Report 2007-1389*, 2007.
26. Hardin, E., Kurum, M., Mitasova, H., and Overton, M., Least cost path extraction of topographic features for storm impact scale mapping, *J. Coastal Res.*, 28(4):970–978, 2012.
27. Ges, V. D. and Starovoitov, V., Distance-based functions for image comparison, *Pattern Recognition Lett.*, 20(2):207–214, 1999.
28. Warren Liao, T., Clustering of time series data-a survey, *Pattern Recogn.*, 38:1857–1874, 2005.
29. Bentley, C. and Ward, M., Animating multidimensional scaling to visualize n-dimensional data sets, In *Proceedings IEEE Symposium on Information Visualization*, pp. 72–73, 1996.
30. Todorovski, L., Cestnik, B., Kline, M., Lavrač, N., and Džeroski, S., Qualitative clustering of short time-series: A case study of firms reputation data, In *Proceedings of ECML/PKDD'02 Workshop on Integration and Collabration Aspects of Data Mining, Decision Support and Meta-Learning*, Helsinki, Helsinki University Printing House, pp. 141–149, 2002.

APPENDIX A. SIMILARITY MEASURES

Table A.1 lists some similarity measures that we have explored to cluster elevation time series in our geospatial data sets.

TABLE A.1: Similarity metrics

Similarity metric	Description
Squared difference	Considers changes in quantities such as elevations, mean elevations, and ratio of elevations and means. This measure is based on the standard Euclidean metric. The full description of the measure is as follows: Given N points that are sampled on a raster map and their elevations $\mathbf{e^i} = (e_0, e_1, \ldots, e_t), i \in [1, N]$ over t time steps, similarity score (D_{ab}) between time series of elevations of two sample points a, b on the terrain is $$D^E_{ab} = \sqrt{\frac{(m^a - m^b)^2}{\texttt{max\_squared\_mean\_diff}}} + \sqrt{\sum_{i=1}^{t}\left(\frac{(e^a_i - e^b_i)^2}{\texttt{max\_squared\_elev\_diff}}\right)} + \sqrt{\sum_{i=1}^{t}\left(\frac{(\frac{e^a_i}{m^a} - \frac{e^b_i}{m^b})^2}{\texttt{max\_squared\_ratio\_diff}}\right)} \quad \text{(A.1)}$$
Qualitative metric	A qualitative metric that compares shapes of time series [30] is $$D^Q_{ab} = \frac{4}{N(N-1)}\sum_{i<j}\mathbf{Diff}[q(a_i, a_j), q(b_i, b_j)] \quad \text{(A.2)}$$ Where $\mathbf{a}, \mathbf{b}$ are the two time series, $q(v_i, v_j)$ denotes qualitative change in the time series v and **Diff** accounts for relative qualitative changes in two different time series (that is, increase, decrease, and no change). See [30] for details.
Pearson correlation	A standard measure of correlation among two data series. $$D^P_{ab} = \frac{1}{N}\sum_{i=1}^{N}\frac{(a_i - \mu^a)(b_i - \mu^b)}{\sigma^a \cdot \sigma^b} \quad \text{(A.3)}$$ Where μ, σ are mean and standard deviation of the two time series $\mathbf{a}, \mathbf{b}$.